Accepted Manuscript

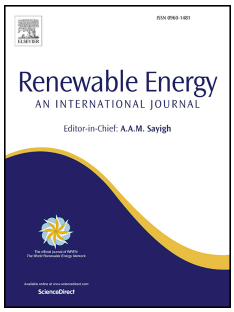

Photovoltaic Evaporative Chimney as a new alternative to enhance solar cooling

M. Lucas, F.J. Aguilar, J. Ruiz, C.G. Cutillas, A.S. Kaiser, P.G. Vicente

PII: S0960-1481(17)30278-1

DOI: 10.1016/j.renene.2017.03.087

Reference: RENE 8680

To appear in: *Renewable Energy*

Received Date: 20 July 2016

Revised Date: 18 January 2017

Accepted Date: 28 March 2017

Please cite this article as: Lucas M, Aguilar FJ, Ruiz J, Cutillas CG, Kaiser AS, Vicente PG, Photovoltaic Evaporative Chimney as a new alternative to enhance solar cooling, *Renewable Energy* (2017), doi: 10.1016/j.renene.2017.03.087.

Photovoltaic evaporative chimney as a new alternative to enhance solar cooling

M. Lucas[a,*], F.J. Aguilar[a], J. Ruiz[a], C.G. Cutillas[a], A.S. Kaiser[b], P.G. Vicente[a]

[a] *Departamento de Ingeniería Mecánica y Energía, Universidad Miguel Hernández, Avda. de la Universidad, s/n, 03202 Elche, Spain*
[b] *Departamento de Ingeniería Térmica y de Fluidos, Universidad Politécnica de Cartagena, Dr. Fleming, s/n, 30202 Cartagena, Spain*

Abstract

Cooling sector plays a crucial role in the World's transition towards an efficient and decarbonised energy system. Solar cooling is an attractive idea because of the chronological coincidence between available solar radiation and cooling needs. This paper studies the possibility of increasing the efficiency of solar photovoltaic modules by evaporative cooling. This, combined with the use of a water condensed chiller, will enable an efficient cooling system design as a whole. To achieve this goal this paper experimentally evaluates the thermal and electrical performance of a Photovoltaic Evaporative Chimney. A prototype with two photovoltaic modules was built; one of them is used as a reference and the other is modified in its rear side including the evaporative solar chimney. The system is able to dissipate a thermal power of about 1500 W with a thermal efficiency exceeding 30% in summer conditions. The module temperature differences reach 8 K, depending on the wind conditions and ambient air psychrometric properties. Regarding the electrical efficiency, the results showed an average improvement of 4.9% to a maximum of 7.6% around midday in a typical summer day for a Mediterranean climate.

Keywords: Solar cooling, Solar chimney, Evaporative cooling, PV/T, Cooling Tower, HVAC

1. Introduction

Heating and cooling constitute around half of the European Union's final energy consumption and is the biggest energy end-use sector, ahead of transport and electricity. Around 85% of heating and cooling is produced from natural gas, coal, oil products and non-RES electricity. Only 15% is generated from renewable energy, (European-Commission, 2015). This shows that the heating and cooling sector has a crucial role to play in the World's transition towards an efficient and decarbonised energy system and in achieving long term energy security. The purpose is to moderate the heating and cooling demand, to increase energy efficiency in supply, to maximise the use of renewable energy and to reduce the cost of heating and cooling to affordable levels.

Although electrically driven chillers have reached a relatively high standard concerning energy consumption, the installed capacity of air conditioning systems has caused an increase of the electricity peak demand in the summer period in many countries. Blackouts and brownouts in summer have frequently been attributed to the large number of conventional cooling systems running on electrical energy. An obvious possibility to counter this trend is to use the same energy for cooling generation that contributes to creating the cooling demand. Solar cooling is an attractive idea because of the chronological coincidence between available solar radiation and cooling needs. The grand challenge is to design solar air conditioning systems in a cost-efficient way. So far, different technical solutions that combine solar energy and air conditioning have been studied.

Solar energy can be converted into cooling using two main principles. Ghafoor and Munir (2015) presented an overview of different available and actually installed solar driven technologies used for cooling or air-conditioning purposes. In Solar Thermal driven Cooling (ST-C), heat generated with solar thermal collectors can be converted into cooling using thermally driven refrigeration or air-conditioning technologies. Most of these systems use the physical phenomena of sorption in either an open or closed thermodynamic cycle. There are several studies where these technologies are exposed and they are developed with flat plate solar collectors or solar vacuum tubes as solar caption surface. Other technologies, such as steam jet cycles or other cycles using a conversion of heat to mechanical energy and of mechanical energy to cooling are less significant. Best and Rivera (2015) presented a review of the performance and development of thermal-powered cooling systems. In Photovoltaic driven Cooling (PV-C), electricity generated with photovoltaic modules can be converted into cooling using well-known refrigeration technologies that are mainly based on vapor compression cycles. In Aguilar et al. (2014) an experimental study with PV-C is described. Also, in Ji et al. (2008) a performance analysis of a PV heat pump is shown.

It is difficult for solar thermal cooling to emerge as a

*Corresponding author. Tel.: +34966658887; fax: +34965222493
Email address: mlucas@umh.es (M. Lucas)

Nomenclature

A_V	Surface area of the water droplets (m^2/m^3)
C_p	Specific heat capacity (J/(kg K))
G_T	Irradiance (W/m^2)
h	Specific enthalpy of moist air (J/kg_a)
h_D	Mass transfer coefficient ($kg/(s\ m^2)$)
$h_{f,w}$	Specific enthalpy of saturated water liquid at T_w (J/kg_w)
$h_{s,w}$	Specific enthalpy of saturated water vapor at T_w (J/kg_w)
I_{mpp}	Nominal current (A)
I_{sc}	Short circuit current (A)
k	Ross coefficient ($K\ m^2/W$)
$\dot{m}$	Mass flow (kg/s)
N	Number of cells
P_{mpp}	Module maximum power (W)
$\dot{Q}$	Cooling power (W)
T	Temperature (°C)
V_{oc}	Open circuit voltage (V)
V_T	Evaporative cooling volume (m^3)
Greek symbols	
α	Temperature coefficient of I_{sc} (%/°C)
β	Temperature coefficient of V_{oc} (%/°C)
β_{ref}	Temperature coefficient of η_{PV} (1/°C)
γ	Temperature coefficient of $P_{\max}$ (%/°C)
η_{PV}	Electrical efficiency
η_T	Thermal efficiency
Subscripts	
1	Water inlet
2	Water outlet
a	Air
amb	Ambient
cond	Condenser
i	Air inlet
int	Air intermediate
out	Air outlet
w	Water
wb	Wet bulb
Abbreviations	
BIPV	Building integrated photovoltaics
NTU	Number of transfer units
PV-C	Photovoltaic driven cooling
PV	Photovoltaic cell
PV/T	Photovoltaic thermal hybrid solar system
RES	Renewable energy source
ST-C	Solar thermal driven cooling

competitive solution due to technical and economic reasons. Technical issues are related to the limitation of the adaptability of the solar thermal cooling technology to a large spectrum of applications due to the presence of important hydraulics (several loops), complexity of the management between solar resource (cooling and heating loads) and overheating risk management between summer and winter seasons (thermal balance of the targeted building). Besides, sorption technology usually uses cooling towers consuming water, chemical treatments and facing legionella development risks. Regarding to economic aspects, the investment cost for solar thermal cooling technology is still significantly high (3 to 5 times more than an equivalent reversible heat pump), especially for small systems.

According to the International Energy Agency-New generation solar cooling & heating systems task 53, (Mugnier et al., 2015), PV driven compression chillers are the most promising and close to market solar solutions today in the case of small to medium units (<50 kW cooling). Until recently, it seemed that solar assisted cooling had best chances for market deployment in cases such as large buildings with central air conditioning systems, because of the unique development of solar thermal cooling solutions. But, with the huge market increase of the cooling equipment in small residential and small commercial sector, and the tremendous decrease in the cost of PV modules, the situation has changed. Recent studies show the great potential of PV cooling, (Fong et al., 2010), but one is still far away from what is achievable.

One of the major problems which is currently limiting the state-of-the-art solar cooling is related to the efficient conversion of solar energy to electricity. The efficiency of photovoltaic systems depends mainly on the cell temperature. The PV module heating reduces its efficiency dramatically, (Schwingshackl et al., 2013). The open-circuit voltage decreases significantly with the increase of PV module temperature (-0,45%/°C for crystalline silicon), while the short cell circuit current increases only between 0,04 and 0,09%/°C (for crystalline silicon). So, these two effects together reduce the maximum available power (and consequently the electrical efficiency) between -0,3 and -0,5%/°C, (Mattei et al., 2006).

Different techniques for reducing PV modules temperature using cooling systems have been found in the literature. Some of them work by passing air or water on the rear surface through channels or ducts, using natural convection or forced convection by a fan, (Teo et al., 2012; Kaiser et al., 2014). The cell temperature of these PV modules is very much influenced by the capability of ventilating this channel. In other studies the PV module is cooled by spraying water on the top surface of the module. This method was used and the results showed an increase in output power in the range of 4 to 10%, (Odeh and Behnia, 2009). Part of this increase is due to refraction of the solar beam in the water layer and the increase in incident radiation. The module temperature dropped significantly to about 20% leading to an increase in the

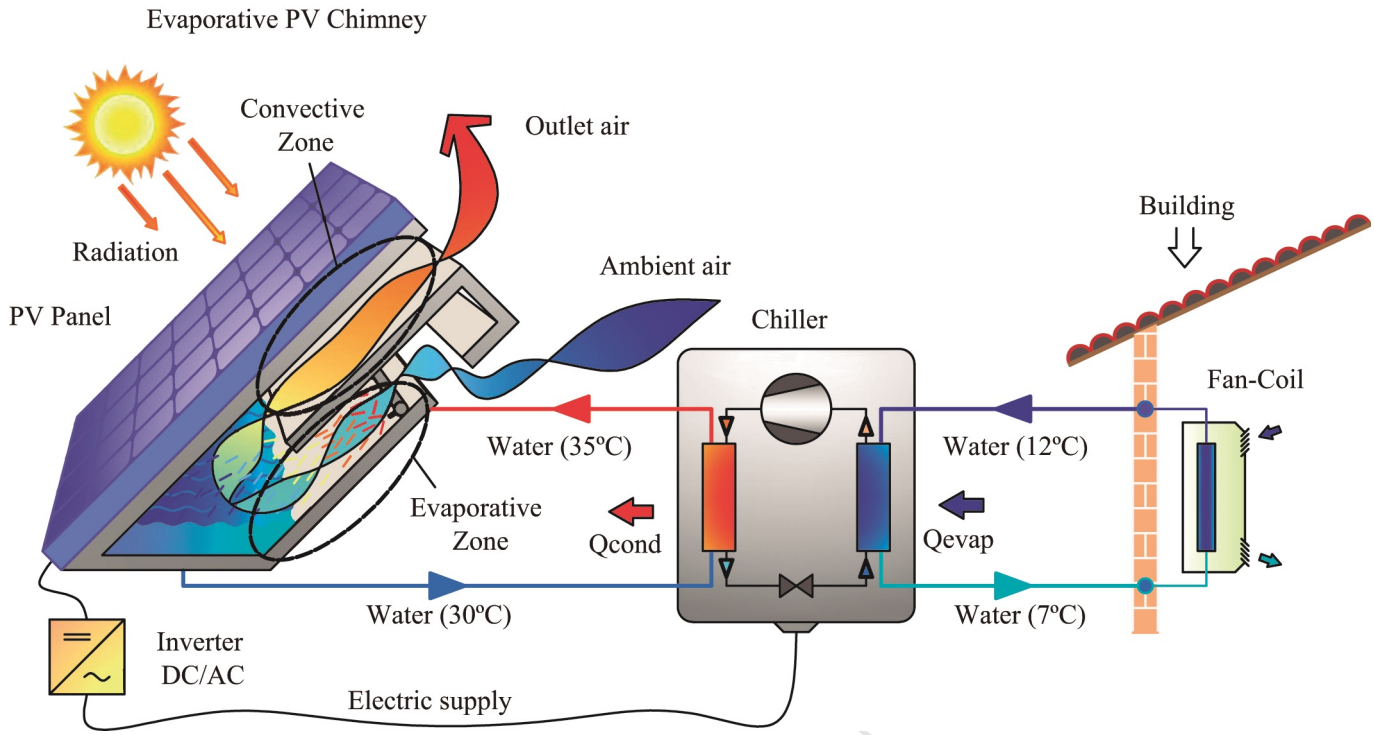

Figure 1: Evaporative PV Solar Chimney and Air conditioning system scheme proposed. Numerical values are included in the drawing for reference only and to facilitate the reader's understanding.

PV module efficiency by 9% with active water cooling, by incorporating a heat exchanger at the rear surface of the module, (Bahaidarah et al., 2013). Sometimes, extracted thermal energy can then be used for heating purposes such as producing domestic hot water in photovoltaic–thermal (PV/T) systems. Reddy et al. (2015) reviewed recent advances in hybrid solar photovoltaic/thermal (PV/T) systems. However, no design has been found in the literature that combines the cooling of the photovoltaic module with condensation of an air conditioning system as the system proposed in this paper.

The second key component of a PV driven compression chiller is the refrigeration equipment. Again, the operating temperature becomes the main variable in determining the performance of the equipment. Commercially, mainly air or water condensed chillers are used. Water-cooled systems use lower levels of temperature in the refrigeration system, so, while maintaining the other operating conditions, energy consumption and cost equipment performance is lower. The effect of decreasing the condensing temperature on the power absorbed by the compressor can be from 1.8 to 4% per degree Celsius, (Yik et al., 2001), depending on the cycle under consideration and the refrigerant used. The best energy efficiency of water-condensed systems is associated with the decrease in CO_2 emissions to the atmosphere. Water-condensed cooling systems usually work with cooling towers or evaporative condensers. Evaporative cooling systems are based on the evaporation of water inside a space, producing lower temperature and higher humidity. The change from liquid to vapor requires energy, which is extracted from the air by cooling it and increasing its humidity. This brings about a change from sensitive heat (drop in temperature) to latent heat (increase in water content in the mix of humid air).

This paper studies the possibility of increasing the efficiency of solar photovoltaic modules by evaporative cooling. This, combined with the use of a water condensed chiller will enable an efficient cooling system design as a whole. To achieve this goal we propose to design a new system that combines evaporative cooling with PV modules, called Photovoltaic Evaporative Chimney, as a new alternative to enhance solar cooling. A Solar Chimney is a thermo-syphoning air channel in which the principal driving mechanism of air flow is through thermal buoyancy. The solar energy causes a temperature rise as well as a density drop in the air inside the solar chimney. The drop in air density causes air within the solar chimney to rise and be expelled out of the top of the chimney, (Zhai et al., 2011). Solar chimneys are applied in different fields such as building ventilation, drying processes, or production of electricity systems, (Zhou et al., 2010). There are some studies about the use of solar chimneys to cool PV modules by means of an airflow, in the same way described above, but they do not include evaporative cooling as in this paper, (Makki et al., 2015). Our group used a solar chimney as a heat sink of a refrigeration cycle however we did not include the possibility of using photovoltaic modules to drive the cooling unit, (Lucas et al., 2006). The main objective of this work is to experimentally evaluate the thermal and electrical performance of a Photovoltaic

Evaporative Chimney prototype for different values of the incident solar radiation and different ambient conditions (ambient temperature and relative humidity).

2. System Description

Figure 2: Prototype of Photovoltaic Evaporative Chimney.

The objectives of the proposed Photovoltaic Evaporative Chimney are two-fold, (see Fig. 1). On the one hand, the system seeks to cool the photovoltaic module and, on the other, to dissipate heat from a refrigeration cycle. To this end, the solar chimney is divided into two main parts. Following the path of the airflow; the first section, called the evaporative cooling zone, has a series of nozzles that spray water parallel to the downward airflow. In this section the heat and mass transfer between water and air occurs. As the water descends, a small part evaporates, cooling the remaining water. This zone works as a small scale cooling tower. The air that has been in contact with water and may have reduced its temperature (it will depend on ambient conditions) then rises up due to buoyancy force through the second part, called the convective zone. Therefore, the second section is basically a solar chimney. The photovoltaic module is cooled by the air stream flowing through the rear and, consequently, an improved performance can be obtained. The working hypothesis for this paper is based on improving the efficiency of photovoltaic modules using evaporative cooling. The water used for cooling the modules will be available to be used for the condensation of a refrigeration cycle.

Magnitude	Units	Value
Maximum Power, P_{mpp}	W	255
Tolerance P_{mpp}	%	0/+3
Dimensions	mm	$1637 \times 992 \times 40$
Number of cells, N		60
Cell Type	156×156 mm	Poly-Crystalline Silicon
Module Efficiency	%	15.7
Short Circuit Current, I_{sc}	A	9.11
Open Circuit Voltage, V_{oc}	V	37.49
Nominal Current I_{mpp}	A	8.44
Nominal Voltage V_{mpp}	V	30.24
Temp. Coeff. of I_{sc}, α	(%/°C)	0.55
Temp. Coeff. of V_{oc}, β	(%/°C)	-0.33
Temp. Coeff. of P_{mpp}, γ	(%/°C)	-0.44

Table 1: Specifications Sunrise module SR-P660255.

3. Method

3.1. Experimental setup

The Photovoltaic Evaporative Chimney prototype was installed on a laboratory roof at the Universidad Miguel Hernández (38 °16'N), Spain. The basis of the solar installation consists of two photovoltaic modules Sunrise, SR-P660255, see specifications on Table 1, arranged as shown in Fig. 2. The module located on the right was used as reference (Module 1) and the module on the left was modified on the back sice including the evaporative solar chimney (Module 2). The orientation for the PV modules is true south (Azimuth angle 0 °) and although the experimental installation is ready to work with 30 °, 45 ° and 60 ° tilt angles, in the present work is fixed at 45 °. The study of the angle influence is left for a future work. In addition, the laboratory building is a freestanding building, so the prototype will not be affected by shadows of other construction elements or facilities except late in the afternoon.

Both PV modules were directly connected to a micro-inverter equipment to convert the direct current produced by the PV modules (24 V) into alternate current (230 V). A grid-tied micro-inverter (APsystems YC500A) with intelligent networking and monitoring systems to ensure maximum efficiency, with a nominal power of 500 W, and independent electrical connection to the modules was used. This equipment was selected because it had an independent maximum power point control for each module, in addition for being perfectly adjusted to the technical characteristics of the PV facility. To dissipate the energy produced by the PV modules, an electrical resistance of 750 W was installed. An electrical inhibitor was connected between the electrical production point and the consumption point, to avoid injecting the electrical energy produced by the PV modules into the grid. Thus, the whole energy produced was self-consumed by the facility. This inhibitor consisted of an Arduino microcontroller capable of processing the information from a clamp ammeter installed on the main wire and adapting the energy consumption by using the electrical resistance in order to avoid the energy injection into the grid.

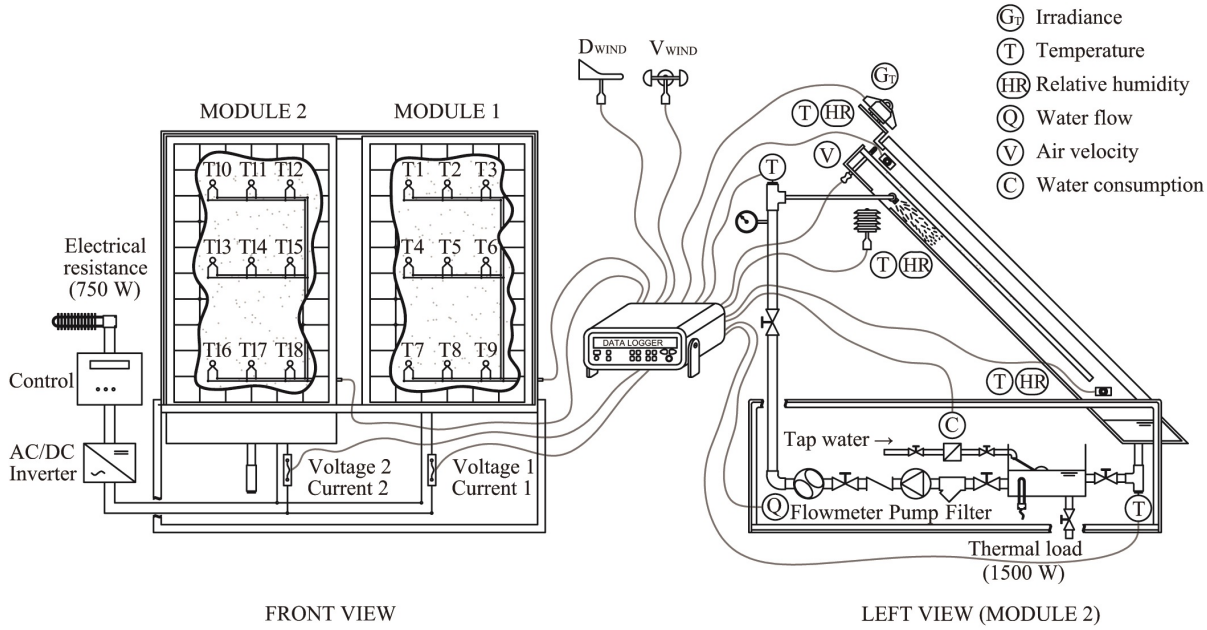

Figure 3: Schematic diagram of the experimental prototype and measurement equipment.

The hydraulic circuit is composed of a network of PVC pipes, see Fig. 3. A pump (ESPA Mod. Prisma 15 3M), recirculates water from the tank to the nozzles arranged linearly in the input section of the solar chimney. The flat spray nozzles (Spraying Systems Co. Mod. ProMax Clip-Eyelet spray angle 110 °) atomize the water evenly. The sprayed water mass flow rate can be changed manually by means of a balancing valve (STAD DN15). An electrical heater (1.5 kW) immersed in the tank is used to simulate the thermal load of the air conditioning machine. A water float ball valve is used to automatically fill the tank and also a filter is included to eliminate all kinds of things that can be harmful entering the pump.

To experimentally analyze the thermal and electrical performance of the Photovoltaic Evaporative Chimney a series of variables were monitored and recorded. The first group of sensors are responsible for measuring environmental conditions: ambient air temperature, air relative humidity, wind speed and wind direction all of them are measured with a meteorological station placed on our laboratory roof just beside the experimental facility. A first class pyranometer installed in the same plane of the PV modules is used to measure radiation. The variables related to the thermal performance of the system are: air temperature and relative humidity measured at the transition point between the evaporating section and the convective section and at the output section, air velocity inside the solar chimney, inlet and outlet water temperatures, water mass flow and water consumption. Nine K-type thermocouples were installed on the rear side of each module distributed in a matrix form to measure the temperature of the PV modules. Regarding electrical parameters, voltages of each are directly measured and the currents of each module are determined from a value of voltage drop produced in a shunt resistance, calibrated to the passage of electric current. A general-purpose data-acquisition system was set up to carry out the experimental tests. All data were monitored with an Agilent 34972 A Data Acquisition Unit with three Agilent 34901 A 20 Channel Multiplexer Modules inserted. A specific measurement data spreadsheet using Benchlink Data Logger 3 was written and compiled for the system, supporting up to 66 inputs, with 16 bits A/D, 9600 bauds transmission speed and programmable gain for each individual channel. The sensors used during the experiment are shown in Fig. 3. The specifications of the measuring devices are presented in Table 2.

3.2. Experimental procedure

Before starting the tests, a calibration step of the measurement system was performed. In order to achieve accurate readings from the 18 thermocouples; it was necessary to calibrate them following a basic calibration process heating water in a thermo bath. Secondly, although the two PV modules were acquired as identical, a calibration process was done to be sure that the measurement of the power generated was the same for both modules. This step led to include a correction curve of the electrical power as a fetion of radiation to match both. After that, tests were carried out throughout 2015-2016, both in summer and winter conditions.

The experimental procedure starts initiating the circulation of the water flow (500 l/h), and switching on the electrical heaters (1.5 kW). In order to achieve steady operating conditions for all the variables, including temperatures, a startup period of 30 minutes was considered. From that moment, the prototype was working from early morn-

Measurement	Brand - Model	Measuring device	Measuring range	Accuracy
Ambient air temperature	E+E Elektronik (EE 21)	Capacitive sensor	-20 - 80°C	±0.3°C
Ambient Air relative humidity	E+E Elektronik (EE 21)	Capacitive sensor	0-100%	±2%
Air temperature	E+E Elektronik (EE 21)	Capacitive sensor	0-100°C	±0.4°C
Air relative humidity	E+E Elektronik (EE 21)	Capacitive sensor	0-100%	±2.5%
Wind direction	Young (05103L)	Balanced vane	0-360°	±3°
Wind Speed	Young (05103L)	4-blade helicoid propeller	0-50 m/s	±2.5 m/s
Water temperature	Desin (ST-FFH Pt100)	4 wires Pt100/RTD	-200-600°C	±0.05°C
Module temperature	RS	K-Type thermocouple	-5-1100°C	±1.5°C
Irradiance	Kipp&Zonen CM-6B	First class pyranometer	0-1400 W/m^2	±1% RD
Water consumption	SENSUS MS8100	Volumetric water meter	0-500 l	±1% RD
Water flow rate	Kronhe Optiflux 1000	Electromagnetic flowmeter	0-2.5 m^3/h	±0.3% RD
Air velocity	E+E (EE65)	Hot film anemometer	0-10 m/s	± (0.2 m/s+3% RD)

Table 2: Measuring equipment used in the experimental prototype and measurement accuracy.

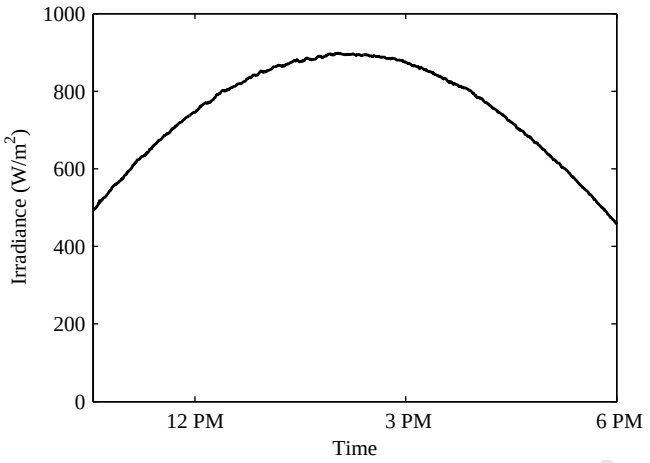

Figure 4: Global irradiance in the module plane (July 10, 2015).

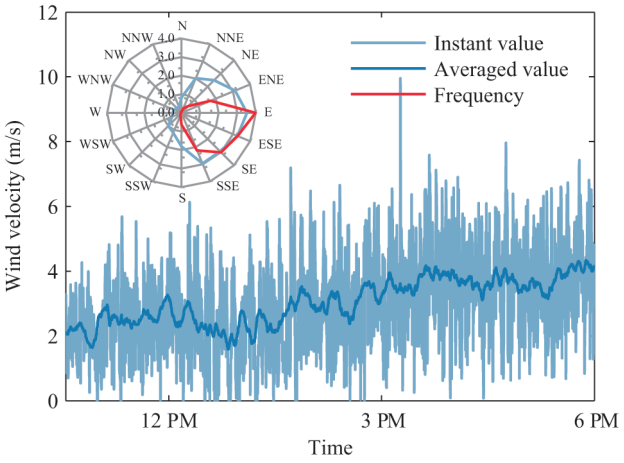

Figure 5: Wind velocity (instant and 10 min averaged) and wind direction (July 10, 2015).

ing until late afternoon. UNE-EN 12975-2 "Thermal solar systems and components - Solar collectors - Part 2: Test methods" and Standard UNE 13741 "Thermal performance acceptance testing of mechanical draught series wet cooling towers" were selected as reference to define stationary conditions. For a test to be valid, variations in the test conditions shall be within the following limits during a 10 minutes period. The variations of the circulating water flow rate shall not be greater than 5%. The maximum deviation of the wet-bulb temperature may not exceed its average value during the test period (±1.5°C). The same is valid for the dry-bulb temperature with a deviation of (±4.5°C) and water temperatures (±1.5°C). The wind velocity shall not exceed 7 m/s for one minute and its average value during the test period shall not exceed 3.5 m/s. Global solar irradiance was over 700 W/m^2 and deviation from the mean less than (± 50 W/m^2).

4. Results and discussion

Different tests were carried out to evaluate the thermal and electrical performance of the Photovoltaic Evaporative Chimney. The results presented in this paper have been recorded over a year in different measurement periods to analyze system behavior in different environmental conditions that occur in a Mediterranean climate. According to the experimental procedure and to comprehensively describe the tests, the results are displayed on three levels: instantaneous measurements (frequency reading 10 s), averaged measurements (each 10 minutes) and stationary intervals. First, results of a clear summer day are shown in detail and after that the trends that were found for other operating conditions are displayed.

4.1. Detailed results: measurements during one day

The presentation and discussion of the results is structured in three parts: first the description of the environmental conditions, then the analysis of the thermal performance of the system and finally the main results of the electrical performance will be presented. Starting with the description of environmental conditions, Fig. 4 shows the results of irradiance on July 10, 2015. As it can be observed, it was a day completely clear in which the irradiance exceeded 900 W/m^2 at noon. Fig. 5 shows measurements of wind velocity, with an average value throughout

the whole day of 3.03 m/s. We note that the wind velocity at the start of the day is medium-low and as the day progresses its value increases with wind gusts exceeding 6 m/s. This is a very common situation at the site of the pilot plant due to the influence of thermal winds from the coast.

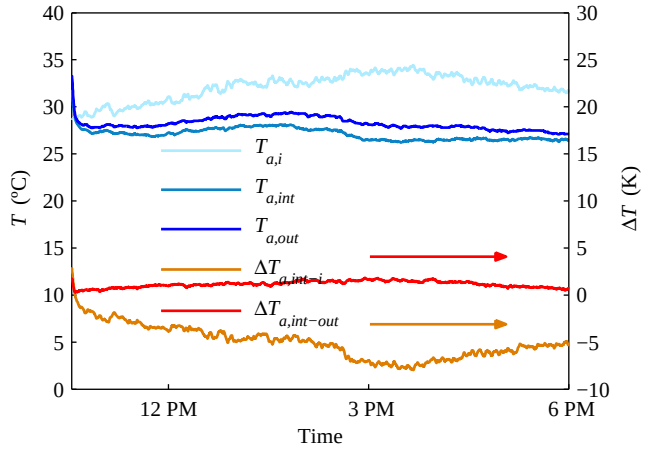

Figure 6: Inlet, Intermediate and Oulet Air Temperature (July 10, 2015).

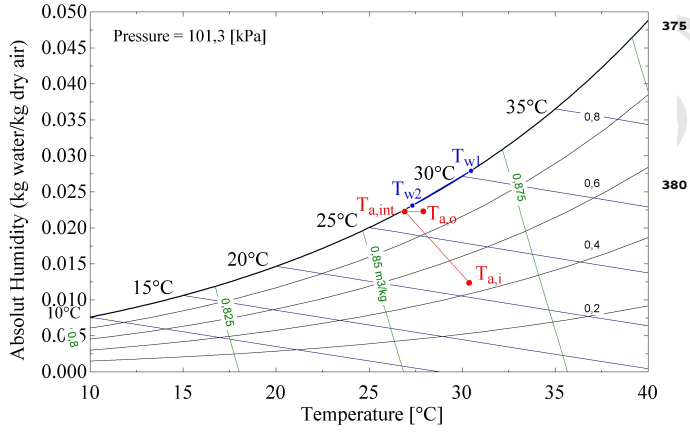

Figure 7: Psychrometric processes.

Fig. 6 shows the experimental results obtained for air temperature in three points: inlet (dry ambient air temperature), intermediate (located just in between the evaporative and convective section) and outlet air temperature. It can be seen that the air temperature drops an average of about 5 K in the evaporative section $\Delta T_{a,\mathrm{int}-i} = T_{\mathrm{int}} - T_i$. In contrast, the air is heated in the convective section acting as a heat sink for the photovoltaic module. It draws attention to the smallest increase in air temperature in the convective zone, however it must be emphasized that the outlet air temperature and relative humidity sensor is located at the midpoint of the outlet section of the convective chimney. This value can be used to ajust the temperature

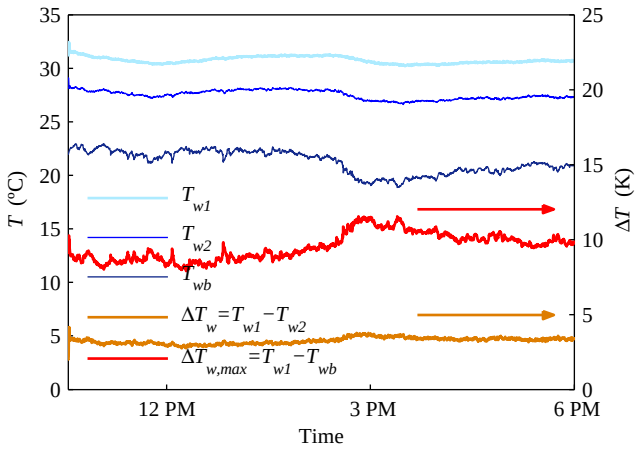

Figure 8: Inlet and outlet water temperature, wet bulb temperature, water temperature difference and temperature difference related to the wet bulb temperature (July 10, 2015).

profile in the thermal boundary layer and therefore the convection heat transfer can be analyzed.

As a low-scale cooling tower, the Photovoltaic Evaporative Chimney cools water by a combination of heat and mass transfer. Baker and Shryock (1961) developed a widely used cooling tower theory. They considered a cooling tower having one square foot of plan area; cooling volume V_T, containing extended water surface per unit volume A_V; and water mass flow rate $\dot{m}_w$ and air mass flow rate $\dot{m}_a$. The water is surrounded by the air and the interface is assumed to be a film of saturated air with an intermediate temperature at the water temperature. Thus, the transfer from the interface to the airstream is proportional to the average enthalpy potential $(h_{s,w} - h)$. Assuming a set of simplifying hypotheses, the steady-state energy and mass balances on an incremental volumen is:

$$-\dot{m}_w \, dh_{f,w} = \dot{m}_a \, dh_a = h_D \, A_V \, V_T \, (h_{s,w} - h) \qquad (1)$$

From the Merkel model, (Haussler et al., 1977), water temperature decrease depends mainly on the incoming air wet-bulb temperature; see air processes on psychrometric chart, Fig. 7. The system's thermal efficiency (η_T) can be defined as the relation between actual water temperature reduction, the one existing between sprayed and drained water, $T_{w_1} - T_{w_2}$, and the water temperature's maximum difference, taking the ambient wet-bulb temperature as the physical limit to the drained water temperature, so:

$$\eta_T = \frac{T_{w_1} - T_{w_2}}{T_{w_1} - T_{wb}} \qquad (2)$$

The data averaged for the whole day offer values of water temperature difference of 3.2 K and the temperature difference related to the wet bulb temperature of 9.5 K, see Fig. 8. Therefore the averaged efficiency was around 34%,

reaching values above 37%. The heat dissipated can be expressed as a function of the water mass flow rate and actual water temperature reduction, see Eq. (3), and is also the energy received by the water from the cooling machine condenser, see Fig. 9. In addition to the thermal load from the electrical heater (1500 W), water receives heat from the pump and due to the temperature difference from the environment through the walls of the hydraulic circuit.

$$\dot{Q}_{\text{cond}} = \dot{m}_w C_p (T_{w_1} - T_{w_2}) \tag{3}$$

The most widely used parameter to define the thermal performance of wet cooling tower is the cooling Number of Transfer Units, NTU. With the help of the NTU, it is possible to compare the thermal performance of different cooling towers or to extrapolate the performance of a cooling tower to operating conditions different to those supplied by the manufacturer or tested. From Eq. (1), the NTU is defined as:

$$\text{NTU} = \frac{h_D\, A_V\, V_T}{\dot{m}_w} = \int_1^2 \frac{-dh_{f,w}}{(h_{s,w} - h)} \tag{4}$$

The integral in the Eq. (4) can be solved numerically. To do that, it is necessary to know the condition line of moist air and the evolution of the water properties throughout the cooling tower. Mohiuddin and Kant (1996) following Tchebyshev's numerical integration method, show the procedure for calculating the cooling tower NTU, defined by Eq. (4), in detail. CTI acceptance test code for water cooling towers, suggests this method to determine the tower characteristic. The calculation procedure is usually displayed for countercurrent flow. Here, the method has been adapted for parallel flows, see Table 3. The comparison between the results obtained in the prototype and those found in the literature for a cooling tower with a pressure water distribution systems type and with a gravity water distribution system are shown in Fig. 10. As it can be seen, the cooling capacity of the Photovoltaic Evaporative Chimney is of the same order of magnitude as that reached in a cooling tower with a splash (gravity) water distribution system, considering that the packing usually installed in cooling tower is not included in the prototype to avoid penalizing the air mass flow rate. The larger heat and mass transfer area caused by the spray is offset by the absence of packing. It must be also taken into account the change in the arrangement of the flow (countercurrent and parallel) when comparing the prototype results with the ones shown in the literature, (Lucas et al., 2009, 2013).

$$\text{NTU} = C_{pw} \frac{t_{w1} - t_{w2}}{4} \sum_{j=1}^{4} \frac{1}{(h_{sw} - h)_j} \tag{5}$$

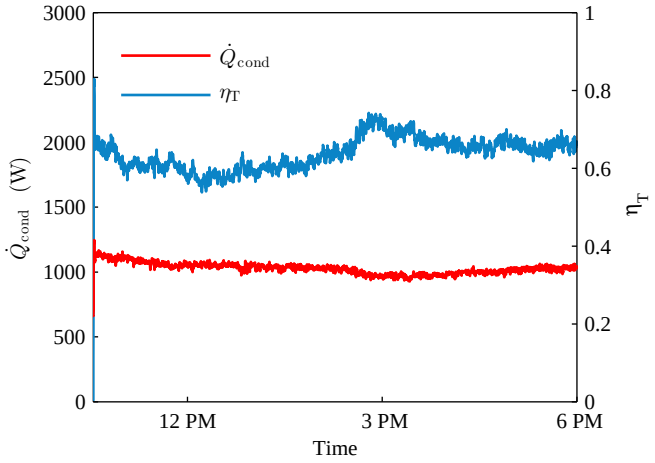

Figure 9: Water Cooling Power and Thermal Efficiency.

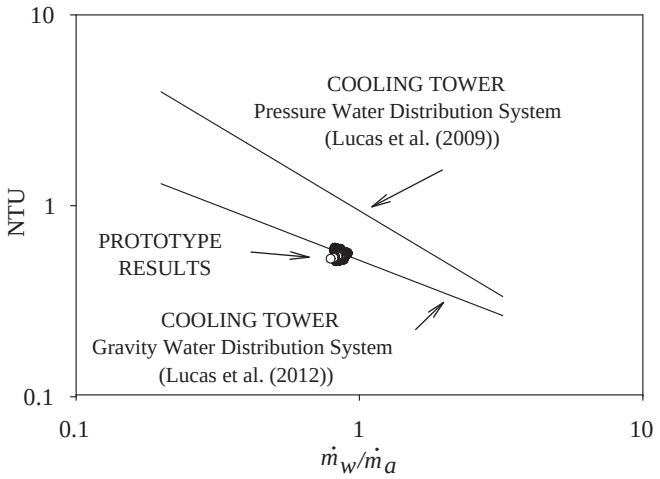

Figure 10: Experimental data of NTU including literature review data from (Lucas et al., 2009, 2013).

t_w	h_{sw}	h	$(h_{sw}-h)_j^{-1}$
t_{w1}		h_1	
$t_A = t_{w1} + 0,1\,(t_{w2}-t_{w1})$	$h_{sw}(t_A)$	$h_A = h_1 + 0,1\,(h_2-h_1)$	$(h_{sw}(t_A)-h_A)_j^{-1}$
$t_B = t_{w1} + 0,4\,(t_{w2}-t_{w1})$	$h_{sw}(t_B)$	$h_B = h_1 + 0,4\,(h_2-h_1)$	$(h_{sw}(t_B)-h_B)_j^{-1}$
$t_C = t_{w1} + 0,6\,(t_{w2}-t_{w1})$	$h_{sw}(t_C)$	$h_C = h_1 + 0,6\,(h_2-h_1)$	$(h_{sw}(t_A)-h_A)_j^{-1}$
$t_D = t_{w1} + 0,9\,(t_{w2}-t_{w1})$	$h_{sw}(t_D)$	$h_D = h_1 + 0,9\,(h_2-h_1)$	$(h_{sw}(t_D)-h_D)_j^{-1}$
t_{w2}		h_2	
			$\sum_{j=1}^{4} \frac{1}{(h_{sw}-h)_j}$

Table 3: Parallel flow NTU Integration.

The next step is to show the graphics related to the temperature reached on the back surface of the photovoltaic modules. First, Fig. 3 shows the location of each of the 18 thermocouples installed in the prototype. The thermocouples responsible for measuring the temperature of the photovoltaic module without chimney (Module 1) are those between T1-T9 and those measuring the module temperature with the chimney (Module 2) are those between T10-T18. It can be verified that the value of the surface temperature is fairly constant for Module 1. In the case of Module 2 a different thermal behavior is observed as there is a temperature stratification. This effect can clearly be seen in Fig. 11 where the temperature values are grouped in triplets by averaging the values of the thermocouples located at the same height on each module (1 to 3, 4 to 6 and so on). It can be seen that the cooling of the module with the chimney is very evident in the lower section with a difference of more than 10°C between the two modules at noon. However, this difference is reduced to about 3.5°C in the middle section and just 1°C in the output section. The module temperature stratification is due to heating the air circulating inside the chimney.

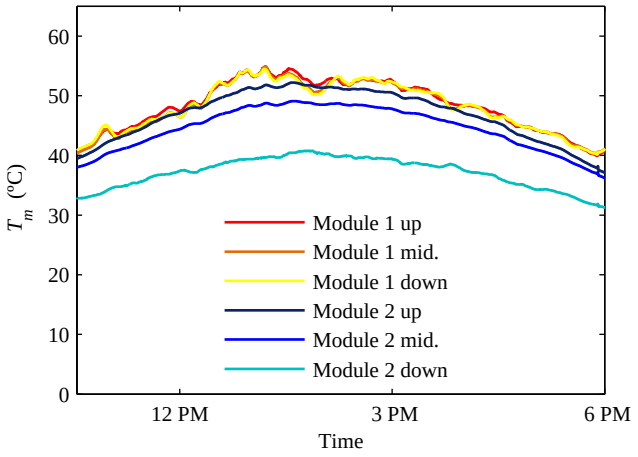

Figure 11: Temperature of the PV modules horizontally averaged.

Fig. 12 shows the rise of the module temperature ($T_m - T_{\text{amb}}$) with respect to the irradiance on the two modules installed in the pilot plant. In order to contextualize the results of our facility with those available in the literature, they are compared with the work of Nordmann and Clavadetscher (2003). The authors analyzed the effect of

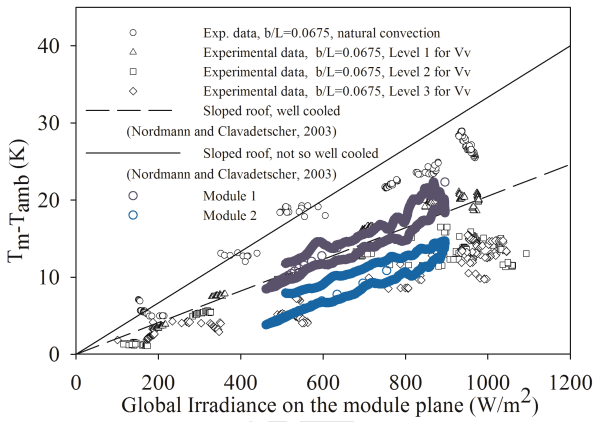

Figure 12: Experimental data of temperature difference between cell and ambient temperature including literature review data from (Nordmann and Clavadetscher, 2003; Kaiser et al., 2014).

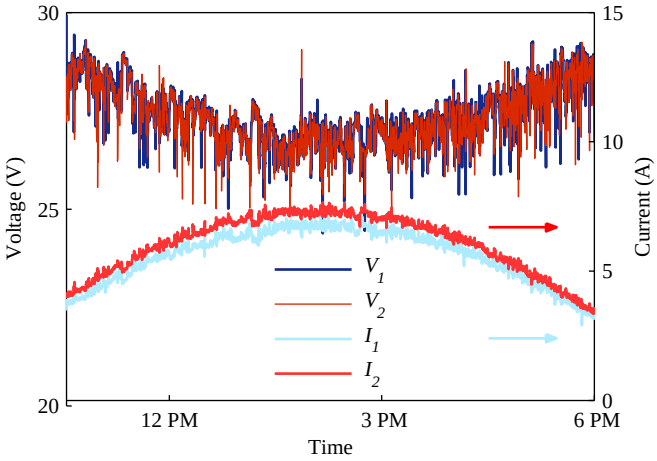

Figure 13: Instant module voltage and current.

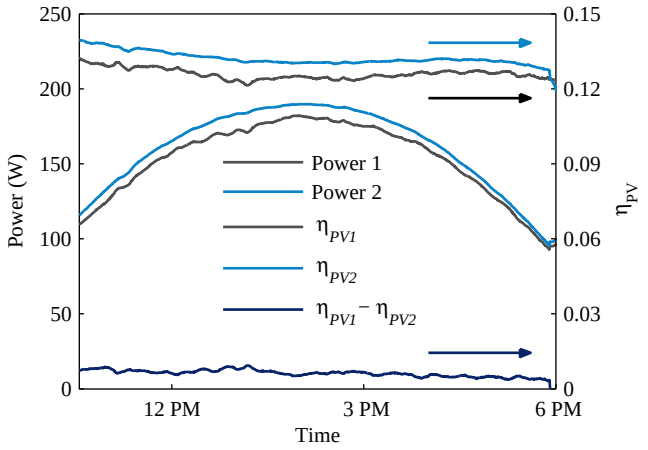

Figure 14: Averaged electrical power and electrical efficiency.

the elevated cell-temperature on the annual performance of PV systems of different mounting (freestanding, roof-mounted and integrated PV façades) from different geographic locations. As it can be seen, the results of Module 1 match with freestanding systems results which usually allow a free airflow around the modules as it might be expected. In addition, a comparison is included with the results of the work of Kaiser et al. (2014). They provided an open air channel beneath the module and study the influence of the air gap size and the forced convection induced by the building ventilation system on the cell temperature of a BIPV configuration. The results show that the temperature of the Module 2 is similar to that of a module with a ventilation of about 5.5 m/s (Level 3 in Fig. 12), despite the averaged outlet air velocity in the prototype is about 2.2 m/s. This is due to the coupled effect between ventilation and air cooling achieved in the evaporative section for the operating conditions shown.

There are two possibilities to model the thermal performance of a PV module. The operating temperature can be correlated by variables that themselves depend on this temperature; where an iteration procedure is necessary for the relevant calculation (the implicit form), or by a correlation that may be solved directly (explicit form). One of the most common explicit expressions employed links the operating temperature with the ambient temperature and the incident solar irradiance, (the slope of the linear correlation of the results in Fig. 12), Ross (1976):

$$T_m = T_{\text{amb}} + k\,G_T \tag{6}$$

The constant k in Eq. (6) (known as the Ross coefficient) denotes the temperature rise above ambient with increasing solar irradiance. Several authors studied the Ross coefficient in different PV configurations from freestanding ($k = 0.021$ K m^2/W) to façade-integrated transparent PV's ($k = 0.046$ K m^2/W) or installed on a sloped roof poorly ventilated ($k = 0.056$ K m^2/W), Skoplaki et al. (2008). For the data measured from the prototype, the average value of Ross coefficient is ($k = 0.025$ K m^2/W) in the case of Module 1 (corresponding with literature values) and ($k = 0.016$ K m^2/W) in Module 2. This shows the good level of cooling that has achieved the proposed design.

In the next paragraph the results related to the electrical performance of the prototype in terms of its main operating variables are discussed: current and voltage, power produced by each module and efficiency obtained. In Fig. 13 instant voltage and current for each photovoltaic module are shown throughout the test period. What makes the difference and indicates which module is being more efficient is the current production, this being higher in the Module 2. Fig. 14 shows the electrical power produced and the efficiency of each module (10 min averaged value). The results show an average value of 12.6% efficiency for the Module 1 and 13.2% for the Module 2. This means

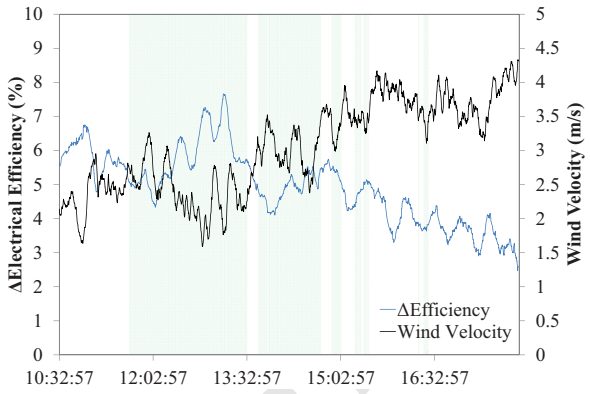

Figure 15: Averaged percentage difference in efficiency and wind velocity. Green shaded areas are stationary intervals.

an average improvement of 4.9% to a maximum of 7.6% around midday. As shown in the graph the efficiency difference is reduced in the afternoon, which is justified by a higher level of wind and a minor temperature difference between modules.

Fig. 15 is used to appreciate more clearly the relationship between increased efficiency achieved and wind speed. As it can be seen, as the wind increases the level of improvement achieved is reduced. When the level of the wind increases, heat transfer to the environment also increases in the module without chimney. This leads to a smaller temperature difference between modules and thus a smaller efficiency difference. In the figure, also, the intervals that meet the stationarity conditions described in the methodology are shown as green shaded areas. These stationary intervals are employed in the next section to describe what happens in different environmental conditions.

4.2. Results for different ambient conditions

This section shows the results of seven tests conducted under different environmental conditions in which have been stationary conditions. While the total number of tests performed was much higher, not always stationary conditions were reached. Therefore, this section only shows the averaged results that met the stationary conditions described in the methodology section. First, Fig. 16 shows the main environmental variables (ambient temperature and irradiance) and the values of the module temperatures to see a summary of the measurement conditions at a glance.

In order to see the influence of the evaporative chimney on the module temperature, Fig. 17 shows the relationship between the temperature of both modules. It can be checked that in the case of module temperatures above 30°C, usually spring-summer conditions, the presence of the chimney leads to a cooler module. This effect is amplified as the temperature of the module increases.

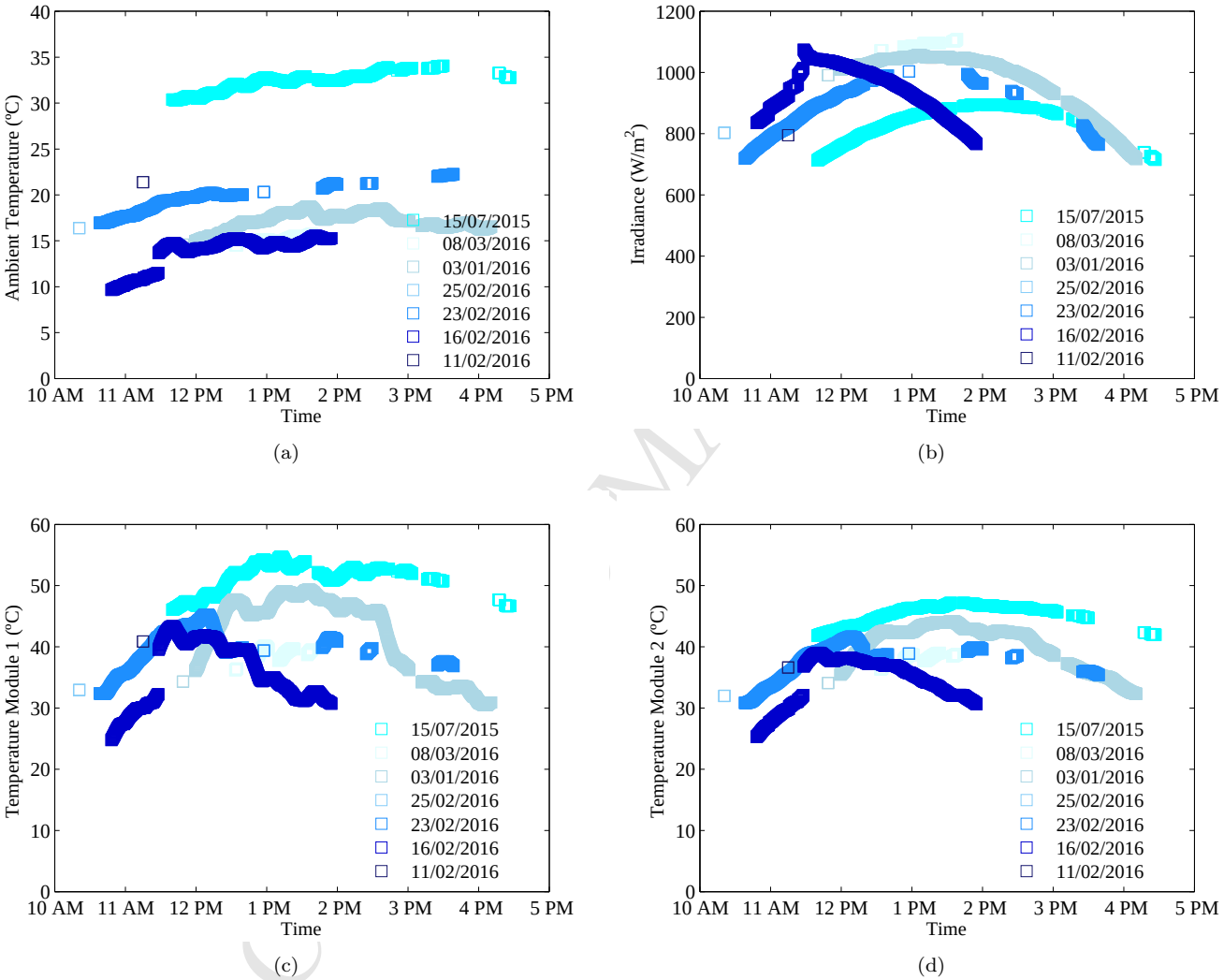

Figure 16: (a) Ambient Temperature; (b) Irradiance; (c) Temperature Module 1; (d) Temperature Module 2.

However, for module temperatures below 30°C, usually in winter conditions, the temperature is quite similar. This is because the psychrometric process of the air into the evaporative section may result in warmer air. There are even days as 03/01/2015, where the temperature of Module 2 is higher than Module 1. To explain in detail the difference between the temperatures of the modules, this is analyzed as a function of the two most influential variables. On the one hand, the difference between the velocity of air inside the chimney and wind velocity is selected since heat dissipation by convection at the back of the modules is dominated by the air velocity. On the other hand the possibility that the air temperature inside the chimney is different from the ambient air is considered due to the psychrometric transformation undergone by the air in the evaporative section. Thus the temperature difference between the intermediate point (start of the convective section) and the ambient temperature is selected. Experimental results show that in cases where the air velocity in the chimney is higher than the wind (v_{out}-$v_{wind} > 0$) and in cases where the difference between the ambient temperature and intermediate temperature is postive (T_{amb}-$T_{int} > 0$); the difference between the temperatures of the modules increases. In quantitative terms it is observed that the difference between measured velocities may be between -1.5 m/s in the case of high wind and get up to 2 m/s in cases where there is low wind. The differences between air temperatures ranging from 4 K air-heating in winter conditions, to 8 K air-cooling in July measures. With this, averaged differences between modules up to 8 K in the most favorable cases are achieved.

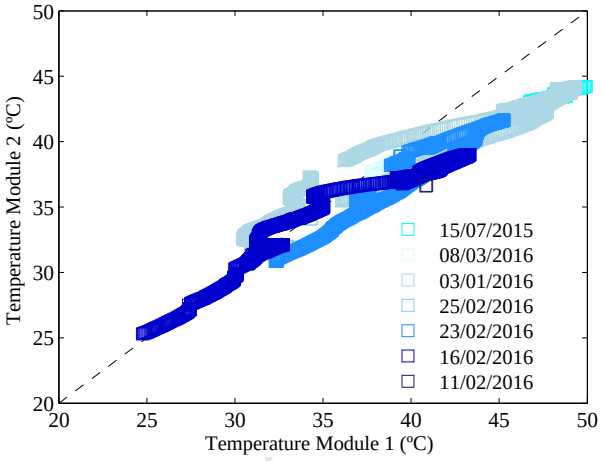

Figure 17: Module 1 and module 2 Temperature Comparison.

Thermal efficiency is used to analyze what happens in the evaporative section. Fig. 18 shows water cooling thermal efficiency at different wet bulb temperatures. It can be observed that the higher the wet bulb temperature, the higher the efficiency, the same occurred in Lucas et al. (2006). As shown in Fig. 18, the efficiency achieved by the system in the measurements made during July exceeds

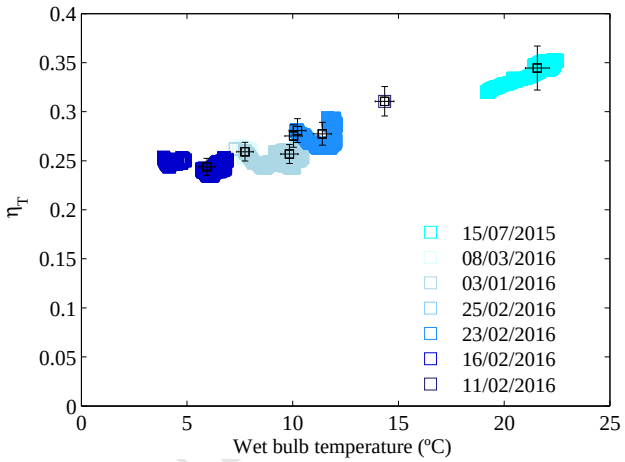

Figure 18: Experimental thermal efficiency for different wet bulb temperatures.

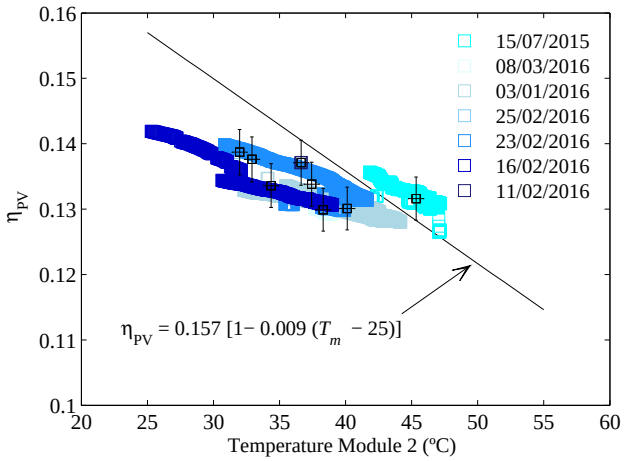

Figure 19: Experimental efficiency measured in the prototype. Experimental correlation based on the traditional linear expression for the PV electrical efficiency.

30%. For these levels of thermal efficiency, it is noted that the outlet water temperature is about 6 K under dry ambient temperature in July. This is one of the key factors in a comparison to evaluate the benefits of Water-Cooled Systems vs. Air-Cooled Systems for Air-Conditioning applications because the lower the condensation temperature, the better the performance. The experimental uncertainty, calculated according to ISO Guide, (ISO, 2004), with a level of confidence of 95% and using sensor specifications shown in Table 2, showed a value of 6.39% and 2.53% for the averaged efficiency and cooling power, respectively. Fig. 18 shows the uncertainty bars in the mean value of each test.

Fig. 19 shows the relationship between the modules temperature and the electrical efficiency. The correlation obtained from the experimental data is included, assuming the traditional linear expression for the PV electrical efficiency, Eq (7). The module's electrical efficiency ($\eta_{\mathrm{PV,ref}}$) at the reference temperature T_{ref} and the efficiency correction coefficient for temperature (β_{ref}) are normally given by the PV manufacturer. However, in this work β_{ref} is deduced from the experimental measurements (see Fig. 19); the estimated values are $\eta_{\mathrm{PV,ref}} = 0.157$ and $T_{\mathrm{ref}} = 25°\mathrm{C}$; and the calculated value for $\beta_{\mathrm{ref}} = 0.0090\ 1/°\mathrm{C}$. The experimental uncertainty showed a value of 2.51% for the electrical efficiency with a level of confidence of 95%.

$$\eta_{\mathrm{PV}} = \eta_{\mathrm{PV,ref}}\left[1 - \beta_{\mathrm{ref}}\ (T_m - T_{\mathrm{ref}})\right] \qquad (7)$$

In the following paragraph, the coupling between the thermal and electrical results is discussed. Fig. 20 shows the percentage improvement obtained in the electrical efficiency of the module with the evaporative chimney with respect to the one that has not been modified. The independent variables selected to show the improvement are those which determine the heat transfer in the module. On the one hand, the difference between ambient and intermediate air temperature is the main variable affecting the efficiency improvement. The greater this difference is, the greater the difference in temperature of the modules and consequently the difference between the electrical efficiencies thereof. On the other hand, the influence of convective flow through the difference between the air velocity inside channel and wind speed has been considered. Again, the greater this difference is, the greater the improvement of the efficiency. Fig. 20 uses a grayscale to show the different ranges of the difference between the air velocity inside channel and wind speed. In view of the results it has been found that the air velocity inside the chimney is affected by the momentum added by the water mass flow at the inlet section, rather than the effect of air buoyancy. On average the level of exhaust air is about 2.4 m/s and the variability for the results is mainly due to the different levels of wind reached. The results show that the effect of the presence of the chimney is negative for the electrical efficiency of the module in winter time. However, the improvement in the electrical efficiency of the module is up to 8% in summer time, when the air conditioning system will usually be used.

5. Conclusions

An environmentally friendly alternative to heat dissipation in buildings and PV electrical production has been experimentally studied. The Photovoltaic Evaporative Chimney as a new alternative to enhance solar cooling increases the electrical efficiency of photovoltaic modules by cooling them and is able to dissipate heat from a refrigeration cycle. The experimental facility consisted of two photovoltaic modules. One of them was used as a reference and the other one was modified in its rear side including the evaporative solar chimney. The experimental results were divided into thermal and electrical performance.

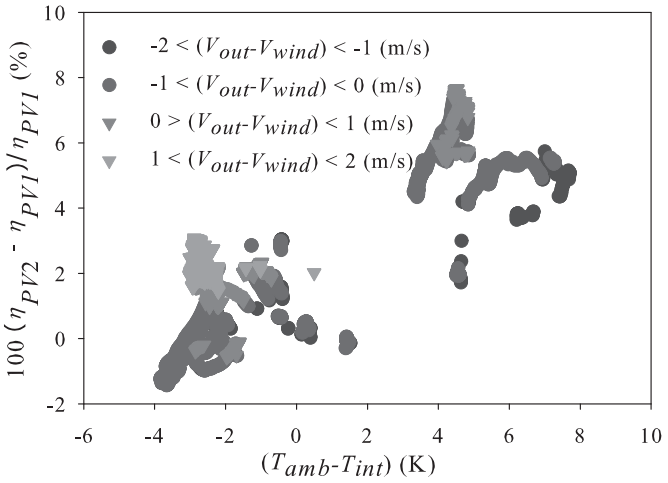

Figure 20: Difference in electrical efficiency of both modules vs $(T_{\mathrm{amb}} - T_{\mathrm{int}})$ and $(V_{\mathrm{out}} - V_{\mathrm{wind}})$.

The parameter used to describe the water cooling capacity of the system was the thermal efficiency, taking the wet bulb temperature as a lower limit. So, the experimental results achieved by the system in the measurements in summer time exceeded a thermal efficiency of 30%. For these levels of thermal efficiency, the outlet water temperature is about 6 K under dry ambient temperature for a heat dissipation of about 1500 W. Coupling between thermal and electrical results is discussed by using the PV module temperature. Cooling of the photovoltaic modules is justified by the air flow and air conditions of entry to the convective section. On the one hand, the difference between the velocity of air inside the chimney and wind velocity, and on the other hand the possibility that the air temperature inside the chimney could be different from the ambient produced up to 8 K of module cooling.

Regarding the electrical efficiency, the results showed an average improvement of 4.9% to a maximum of 7.6% around midday in a typical summer day for a Mediterranean climate. For a comprehensive energy analysis of

the improvements produced by the system, it will be necessary to model it and include it in a simulation program. We have already taken the first steps modelling the PV electrical efficiency by using the traditional linear expression and the evaporative cooling process by using efficiency and NTU, but further analysis is left for future work.

6. Acknowledgements

The authors wish to acknowledge the collaboration in the experimental work of the following Mechanical and Electrical Engineering students: S. Rodríguez, J.F. Bernal, P. Díez, H. Garcés, C. Selva, V. García, J. Navas and E. Gálvez; and especially to E. Sánchez for his amazing work as a lab technician.

References

Aguilar, F. J., Quiles, P. V., Aledo, S., 2014. Operation and energy efficiency of a hybrid air conditioner simultaneously connected to the grid and to photovoltaic panels. Energy Procedia 48, 768 – 777, proceedings of the 2nd International Conference on Solar Heating and Cooling for Buildings and Industry (SHC 2013).
URL http://www.sciencedirect.com/science/article/pii/S1876610214003518

Bahaidarah, H., Subhan, A., Gandhidasan, P., Rehman, S., 2013. Performance evaluation of a pv (photovoltaic) module by back surface water cooling for hot climatic conditions. Energy 59 (C), 445–453.
URL http://EconPapers.repec.org/RePEc:eee:energy:v:59:y:2013:i:c:p:445-453

Baker, D., Shryock, H. A., 1961. A comprehensive approach to the analysis of cooling tower performance. J. Heat Transfer 83 (3), 339 – 349.
URL http://heattransfer.asmedigitalcollection.asme.org/article.aspx?articleid=1432350

Best, R., Rivera, W., 2015. A review of thermal cooling systems. Applied Thermal Engineering 75, 1162 – 1175.
URL http://www.sciencedirect.com/science/article/pii/S1359431114006802

European-Commission, 2015. Horizon 2020 work programme 2016-17. 'secure, clean and efficient energy'.
URL https://ec.europa.eu/programmes/horizon2020/en/h2020-section/secure-clean-and-efficient-energy

Fong, K., Chow, T., Lee, C., Lin, Z., Chan, L., 2010. Comparative study of different solar cooling systems for buildings in subtropical city. Solar Energy 84 (2), 227 – 244.
URL http://www.sciencedirect.com/science/article/pii/S0038092X09002667

Ghafoor, A., Munir, A., 2015. Worldwide overview of solar thermal cooling technologies. Renewable and Sustainable Energy Reviews 43, 763 – 774.
URL http://www.sciencedirect.com/science/article/pii/S1364032114010120

Haussler, W., Stadt, K., OHIO., F. T. D. W.-P. A., 1977. Merkel Theory of Evaporative Cooling.

ISO, 2004. Guide to the expression of uncertainty in measurement (GUM)-Supplement 1: Numerical methods for the propagation of distributions. Vol. ISO draft guide DGUIDE99998. International Organization for Standardization, Geneva.

Ji, J., Liu, K., tai Chow, T., Pei, G., He, W., He, H., 2008. Performance analysis of a photovoltaic heat pump. Applied Energy 85 (8), 680 – 693.
URL http://www.sciencedirect.com/science/article/pii/S0306261908000184

Kaiser, A., Zamora, B., Mazón, R., García, J., Vera, F., 2014. Experimental study of cooling bipv modules by forced convection in the air channel. Applied Energy 135, 88 – 97.
URL http://www.sciencedirect.com/science/article/pii/S0306261914008903

Lucas, M., Kaiser, A., Viedma, A., Zamora, B., 2006. Energy optimization of air conditioning system using hydrosolar roof as a heat sink. Solar Energy 80 (4), 448 – 458.
URL http://www.sciencedirect.com/science/article/pii/S0038092X05001891

Lucas, M., Martínez, P., Viedma, A., 2009. Experimental study on the thermal performance of a mechanical cooling tower with different drift eliminators. Energy Conversion and Management 50 (3), 490 – 497.
URL http://www.sciencedirect.com/science/article/pii/S0196890408004512

Lucas, M., Ruiz, J., Martínez, P. J., Kaiser, A. S., Viedma, A., Zamora, B., 2013. Experimental study on the performance of a mechanical cooling tower fitted with different types of water distribution systems and drift eliminators. Applied Thermal Engineering 50 (1), 282 – 292.
URL http://www.sciencedirect.com/science/article/pii/S1359431112004516

Makki, A., Omer, S., Sabir, H., 2015. Advancements in hybrid photovoltaic systems for enhanced solar cells performance. Renewable and Sustainable Energy Reviews 41, 658 – 684.
URL http://www.sciencedirect.com/science/article/pii/S1364032114007552

Mattei, M., Notton, G., Cristofari, C., Muselli, M., Poggi, P., 2006. Calculation of the polycrystalline {PV} module temperature using a simple method of energy balance. Renewable Energy 31 (4), 553 – 567.
URL http://www.sciencedirect.com/science/article/pii/S096014810500073X

Mohiuddin, A., Kant, K., 1996. Knowledge base for the systematic design of wet cooling towers. part ii: Fill and other design parameters. International Journal of Refrigeration 19 (1), 52 – 60.
URL http://www.sciencedirect.com/science/article/pii/0140700795000607

Mugnier, D., Fedrizzi, R., Thygesen, R., Selke, T., 2015. New generation solar cooling and heating systems with {IEA} {SHC} task 53: Overview and first results. Energy Procedia 70, 470 – 473, international Conference on Solar Heating and Cooling for Buildings and Industry, {SHC} 2014.
URL http://www.sciencedirect.com/science/article/pii/S1876610215002714

Nordmann, T., Clavadetscher, L., 2003. Understanding temperature effects on pv system performance. In: Photovoltaic Energy Conversion, 2003. Proceedings of 3rd World Conference on. Vol. 3. IEEE, pp. 2243–2246.

Odeh, S., Behnia, M., 2009. Improving photovoltaic module efficiency using water cooling. Heat Transfer Engineering 30 (6), 499–505.
URL http://dx.doi.org/10.1080/01457630802529214

Reddy, S. R., Ebadian, M. A., Lin, C.-X., 2015. A review of pvt systems: Thermal management and efficiency with single phase cooling. International Journal of Heat and Mass Transfer 91, 861 – 871.
URL http://www.sciencedirect.com/science/article/pii/S0017931015304002

Ross, R., 1976. Interface design considerations for terrestrial solar cell modules. Proceedings of the 12th IEEE Photovoltaic Specialists Conference, 801 – 806.

Schwingshackl, C., Petitta, M., Wagner, J., Belluardo, G., Moser, D., Castelli, M., Zebisch, M., Tetzlaff, A., 2013. Wind effect on {PV} module temperature: Analysis of different techniques for an accurate estimation. Energy Procedia 40, 77 – 86.
URL http://www.sciencedirect.com/science/article/pii/S1876610213016044

Skoplaki, E., Boudouvis, A., Palyvos, J., 2008. A simple correlation

for the operating temperature of photovoltaic modules of arbitrary mounting. Solar Energy Materials and Solar Cells 92 (11), 1393 – 1402.
URL http://www.sciencedirect.com/science/article/pii/S0927024808001918

Teo, H., Lee, P., Hawlader, M., 2012. An active cooling system for photovoltaic modules. Applied Energy 90 (1), 309 – 315, energy Solutions for a Sustainable World, Special Issue of International Conference of Applied Energy, ICA2010, April 21-23, 2010, Singapore.
URL http://www.sciencedirect.com/science/article/pii/S0306261911000201

Yik, F., Burnett, J., Prescott, I., 2001. Predicting air-conditioning energy consumption of a group of buildings using different heat rejection methods. Energy and Buildings 33 (2), 151 – 166.
URL http://www.sciencedirect.com/science/article/pii/S0378778800000943

Zhai, X., Song, Z., Wang, R., 2011. A review for the applications of solar chimneys in buildings. Renewable and Sustainable Energy Reviews 15 (8), 3757 – 3767.
URL http://www.sciencedirect.com/science/article/pii/S1364032111002498

Zhou, X., Wang, F., Ochieng, R. M., 2010. A review of solar chimney power technology. Renewable and Sustainable Energy Reviews 14 (8), 2315 – 2338.
URL http://www.sciencedirect.com/science/article/pii/S1364032110001292

HIGHLIGHTS:

- The paper evaluates the thermal and electrical performance of a Photovoltaic Evaporative Chimney.
- An evaporative thermal efficiency exceeding 30% in summer conditions has been measured
- An electrical efficiency improvement of 4.9% could be reached on a typical summer day